An ultrathin integrated nanoelectromechanical transducer based on hafnium zirconium oxide

Mayur Ghatge, Glen Walters, Toshikazu Nishida, and Roozbeh Tabrizian **

Nanomechanical resonators that can operate in the super high frequency (3-30 GHz) or the extremely high frequency (30-300 GHz) regime could be of use in the development of stable frequency references, wideband spectral processors and high-resolution resonant sensors. However, such operation requires the dimensions of the mechanical resonators to be reduced to tens of nanometres, and current devices typically rely on transducers, for which miniaturization and chip-scale integration are challenging. Here, we show that integrated nanoelectromechanical transducers can be created using 10-nm-thick ferroelectric hafnium zirconium oxide ($Hf_{0.5}Zr_{0.5}Q_2$) films. The transducers are integrated on silicon and aluminium nitride membranes, and can yield resonators with frequencies from 340 kHz to 13 GHz and frequency-quality-factor products of up to 3.97 \times 10¹². Using electrical and optical probes, we show that the electromechanical transduction behaviour of the $Hf_{0.5}Zr_{0.5}Q_2$ film is based on the electrostrictive effect, and highlight the role of nonlinear electromechanical scattering in the operation of the resonator.

ntegrated nanoelectromechanical transducers allow sensors and actuators to be miniaturized, leading to nanoscale devices with ultrahigh resolution¹⁻³. They could also potentially allow high-frequency and high-quality-factor (Q) mechanical resonances to be harnessed in semiconductor nanostructures, providing stable frequency references, wideband spectral processors and high-resolution resonant sensors in the centimetre-wave regime (super high frequency; SHF) and millimetre-wave regime (extremely high frequency; EHF)^{4,5}. However, the realization of these systems is currently hindered by the scaling limitations of integrated electromechanical resonators. The available mechanical frequency reference, filter and resonant sensor technologies typically rely on microscale resonators that use capacitive gaps^{6,7} or piezoelectric film transducers^{8,9}, and operate over low frequency (LF) to ultra high frequency (UHF) regimes. However, to operate over SHF and EHF regimes, the dimensions of the mechanical resonators need to be reduced to tens of nanometres: nearly two orders of magnitude smaller than available devices. Such scaling is impeded by substantial fabrication limitations of ultra-narrow gaps and ultrathin piezoelectric films to provide integrated transduction at the nanoscale. Shrinking of capacitive gaps and conventional piezoelectric film transducers below 20 nm also markedly reduces their electromechanical transduction efficiency^{10,11}.

High-Q nanomechanical resonators based on two-dimensional crystals such as graphene and molybdenum disulfide have been extensively studied using non-integrated transduction schemes and have demonstrated strong potential for extreme frequency scaling 12-17. However, the absence of a compatible integrated nanoelectromechanical transduction technology prevents the development of monolithic frequency references, spectral processors and resonant sensors. The efficient integration of two-dimensional crystals with complementary metal-oxide-semiconductor (CMOS) technology also remains a significant issue.

Ultrathin hafnium dioxide films have recently emerged as a new class of atomic-layered films that can be engineered to provide enhanced ferroelectric properties^{18–20}. The films can be deposited using a fully CMOS-compatible fabrication process, and have so far been explored for their potential use in the development of low-power and miniaturized non-volatile memory devices.

In this article, we show that ferroelectric hafnium zirconium oxide (Hf_{0.5}Zr_{0.5}O₂) thin films can be used to create integrated nanoelectromechanical transducers via the nonlinear electrostrictive effect. Hf_{0.5}Zr_{0.5}O₂ layers as thin as 10 nm are integrated on silicon (Si) and aluminium nitride (AlN) membranes. The resulting nanomechanical resonators offer frequencies (f_0) from 340 kHz to 13 GHz and f_0Q product up to 3.97×10^{12} , surpassing the of two-dimensional-crystal nanomechanical resonators with similar thickness scales. With the development of devices based on the direct integration of atomic-layered Hf_{0.5}Zr_{0.5}O₂ on Si, we help resolve uncertainties surrounding the dominant producer of the electromechanical transduction effect that were caused by the presence of AlN piezoelectric film in Hf_{0.5}Zr_{0.5}O₂-on-AlN devices²¹. Using electrical and optical probes, we also demonstrate and quantify the role of the nonlinear electrostrictive effect in the electromechanical transduction behaviour of the Hf_{0.5}Zr_{0.5}O₂ film.

Atomic engineering of Hf_{0.5}Zr_{0.5}O₂ thin films

Ultrathin Hf_{0.5}Zr_{0.5}O₂ is known to have various stable and metastable crystal phases^{22,23}. Among these, the non-centrosymmetric orthorhombic metastable phase provides unique ferroelectric properties^{24–27}. While Hf_{0.5}Zr_{0.5}O₂ films grown by atomic layer deposition are amorphous in nature due to the low thermal budget of the growth process, the use of a titanium nitride (TiN) capping layer and application of rapid thermal annealing (RTA) on the stack promotes the dominant growth of the ferroelectric orthorhombic texture. Figure 1 demonstrates the cross-sectional transmission electron microscopy (XTEM) image of the TiN-on-Hf_{0.5}Zr_{0.5}O₂ stack (Fig. 1a), the fast Fourier transform of the atomic diffraction pattern, highlighting the predominant orthorhombic crystal phase after RTA (Fig. 1b), and the ferroelectric-polarization-electric-field characteristic (Fig. 1c), directly measured after RTA and the wakeup process. The TiN-on-Hf_{0.5}Zr_{0.5}O₂ stack is deposited on two substrates with (a) 70 nm single-crystal Si thickness and (b) a 320 nm stack of sputtered hexagonal AlN, molybdenum and Si. The two substrates are used for fabrication of various mechanical resonators operating in bulk and flexural modes of vibration. Microfabrication

NATURE ELECTRONICS ARTICLES

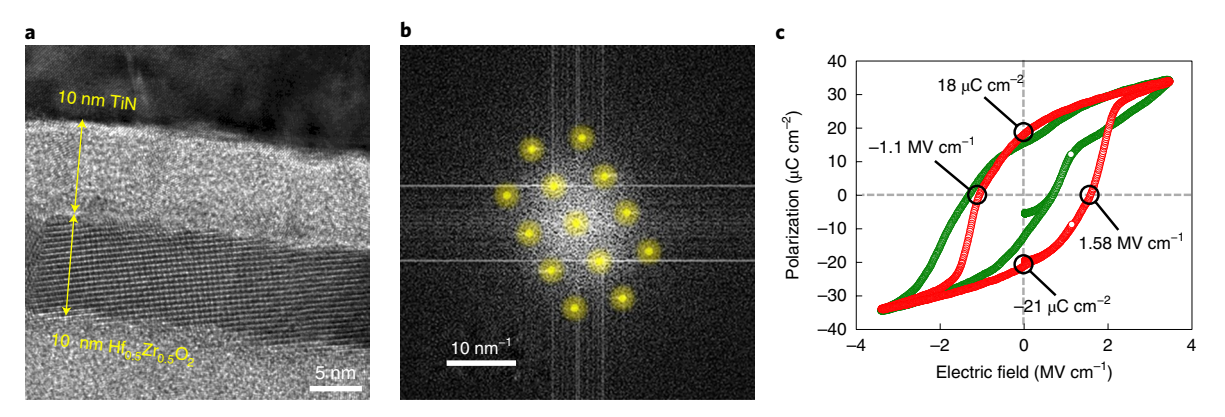


Fig. 1 Atomically engineered polycrystalline $Hf_{0.5}Zr_{0.5}O_2$ with predominant orthorhombic crystal phase. **a**, XTEM image of a TiN-on- $Hf_{0.5}Zr_{0.5}O_2$ stack showing the atomic diffraction pattern of the polycrystalline 10 nm film. **b**, Fast Fourier transform of the ultrathin $Hf_{0.5}Zr_{0.5}O_2$ film showing the predominant orthorhombic crystal phase. **c**, Measured polarization-electric-field characteristic of the $Hf_{0.5}Zr_{0.5}O_2$ film after RTA (green curve) and after the subsequent wake-up process (red curve) showing the hysteresis behaviour corresponding to the ferroelectric effect.

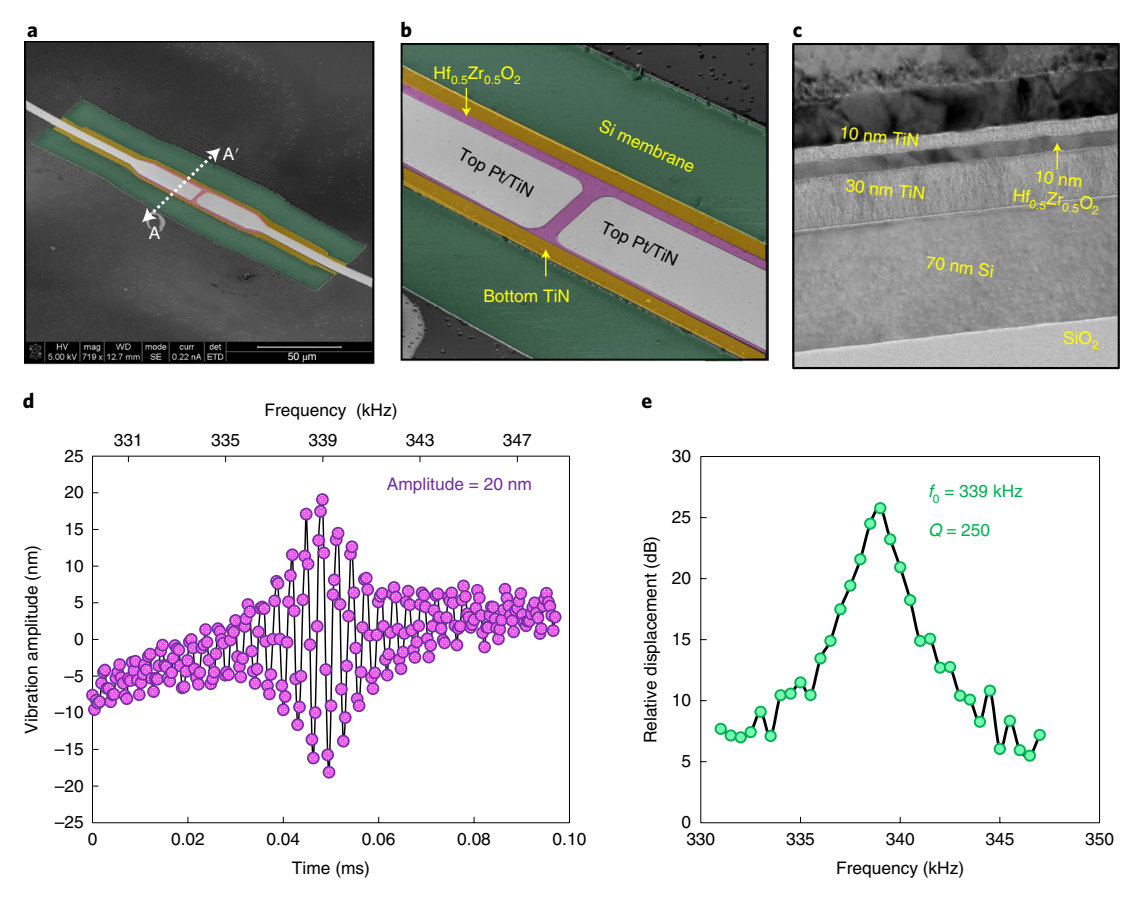


Fig. 2 | A 339 kHz Hf_{0.5} $Zr_{0.5}O_2$ -transduced Si membrane resonator. **a**, SEM image of the Hf_{0.5} $Zr_{0.5}O_2$ -transduced Si nanomechanical resonator operating in out-of-plane flexural mode (the cross-sectional schematic of the device along AA' is shown in Supplementary Fig. 2). **b**, Magnified SEM of the resonator around the Pt/TiN top electrodes used for application of stroboscopic a.c. voltage. **c**, XTEM image of the resonator showing the thickness of the transducer and Si layers. **d**, Stroboscopic vibration analysis using an optical probe at the centre of the resonator, showing a vibration amplitude of ~20 nm at resonance. **e**, The frequency response of the Hf_{0.5} $Zr_{0.5}O_2$ -transduced Si resonator extracted from stroboscopic analysis, showing the flexural resonance at 339 kHz and a Q of 250 in air.

processes including photolithography, reactive-ion and wet-etching processes and deposition of platinum electrodes are exploited to realize free-standing membranes and electrical probing pads

to access the $10\,\mathrm{nm}$ Hf $_{0.5}\mathrm{Zr}_{0.5}\mathrm{O}_2$ integrated nanoelectromechanical transducer (see Supplementary Section 1A for fabrication and processing details).

ARTICLES NATURE ELECTRONICS

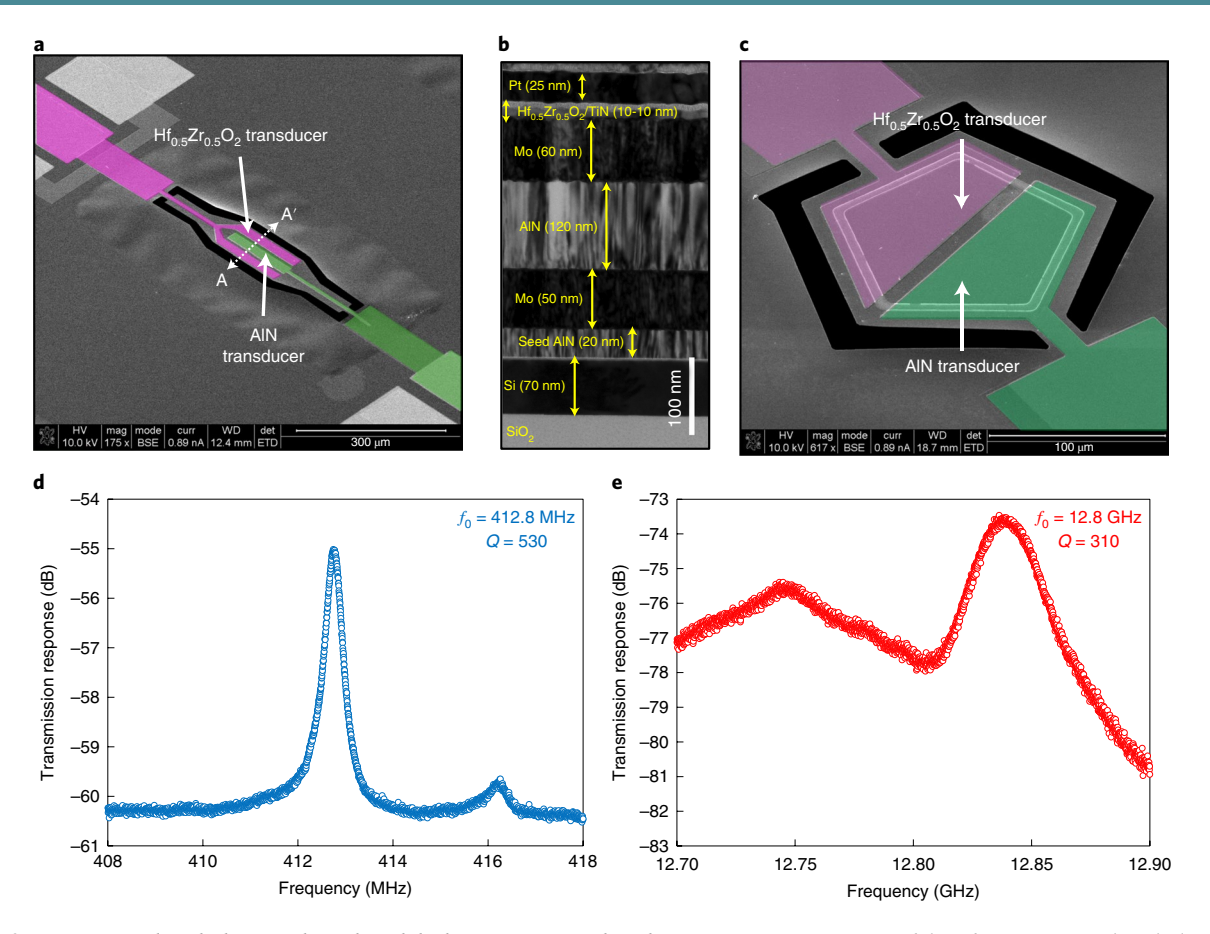


Fig. 3 | $Hf_{0.5}Zr_{0.5}O_2$ -transduced AlN-on-Si lateral- and thickness-extensional mode resonators. **a**, SEM image of the $Hf_{0.5}Zr_{0.5}O_2$ -transduced AlN-on-Si resonator operating in in-plane extensional mode. The cross-sectional schematic of the device along AA' is shown in Supplementary Fig. 3. **b**, XTEM image of the $Hf_{0.5}Zr_{0.5}O_2$ -transduced AlN-on-Si resonator showing the thicknesses of the different layers in the stack. **c**, SEM image of the $Hf_{0.5}Zr_{0.5}O_2$ -transduced AlN-on-Si resonator operating in thickness-extensional mode. **d**, Frequency response of the resonator in **a**, operating at 412.8 MHz with a Q of 530. **e**, Frequency response of the resonator in **c**, operating at a centimetre-wave frequency of 12.8 GHz, with a f_0Q product of 3.97 \times 10¹².

Resonators with $Hf_{0.5}Zr_{0.5}O_2$ integrated transducers

Various resonators operating in flexural and extensional mechanical resonance modes over the 340 kHz to 13 GHz frequency range are demonstrated. In these devices, the Hf_{0.5}Zr_{0.5}O₂ transducers are polarized through application of 3.5 V d.c. for ~1 s to provide linear electromechanical transduction (see Supplementary Section 1B for further details on poling) on insertion of a.c. signal. Figure 2 shows the scanning electron microscopy (SEM) and XTEM images of the $Hf_{0.5}Zr_{0.5}O_{2}$ -transduced Si resonator. This device is excited through application of stroboscopic voltage signal across the $Hf_{0.5}Zr_{0.5}O_2$ film, and the flexural resonance vibration at 339 kHz is detected using a holographic optical probe (see Supplementary Section 1C for further details on device characterization). A Q of 250 is extracted, while operating in air at room temperature. Figure 3 shows the SEM and XTEM images of two UHF and SHF (0.3-30 GHz) Hf_{0.5}Zr_{0.5}O₂transduced resonators implemented in an AlN-on-Si platform, and their frequency response. The 120 nm AlN piezoelectric transducer is used along with the 10 nm Hf_{0.5}Zr_{0.5}O₂ to enable two-port electrical transmission characterization of the resonators operating in UHF and SHF regimes. Figure 3a,c shows resonators operating in lateral- and thickness-extensional modes, with XTEM of the resonator stack shown in Fig. 3b. In these devices, the AlN film is used for actuation and the 10 nm Hf_{0.5}Zr_{0.5}O₂ film is used for electrical detection of the mechanical strain at resonance. The resonator in Fig. 3a operates in the third width-extensional resonance mode at 413 MHz with a Q of 530. The resonator shown in Fig. 3c operates in the thickness-extensional mode, where the resonance frequency

is defined by the thickness of the resonator stack. The resonator shows a Q of 310 at 12.8 GHz, yielding the large f_0Q figure of merit of 3.97×10^{12} (see Supplementary Section 3 for comparison of the f_0Q figure of merit with other reported nanomechanical resonators).

Electrostrictive effect in Hf_{0.5}Zr_{0.5}O₂ transducers

To gain insight and quantitative understanding of the electrome-chanical transduction physics in $Hf_{0.5}Zr_{0.5}O_2$ film, an experimental investigation is performed, and results are compared with an analytical model. The electromechanical transduction in bulk ferroelectric materials is known to be based on the electrostrictive effect²⁸. In this inherently nonlinear effect, the relation between polarization-induced mechanical strain (ε_i) and the dielectric spontaneous polarization (P_i) of the ferroelectric material is defined by

$$\varepsilon_i = Q_{ij} (P_j(\mathbf{E}))^2 \tag{1}$$

Here, Q_{ij} are the electrostrictive coefficients, and P_{j} is related to the electric-field vector (E) through the characteristic polarization–electric-field hysteresis loop. To identify the contribution of the nonlinear electrostrictive effect in atomically engineered $\mathrm{Hf_{0.5}Zr_{0.5}O_2}$ transducers, the resonator in Fig. 2 is driven into mechanical resonance while changing a d.c. bias voltage ($V_{\mathrm{d.c.}}$) along with the a.c. stroboscopic signal.

Figure 4a elucidates the variation of the frequency response of the $Hf_{0.5}Zr_{0.5}O_2$ -transduced Si resonator, around the out-of-plane flexural resonance mode, with different $V_{d.c.}$ over the range from

NATURE ELECTRONICS ARTICLES

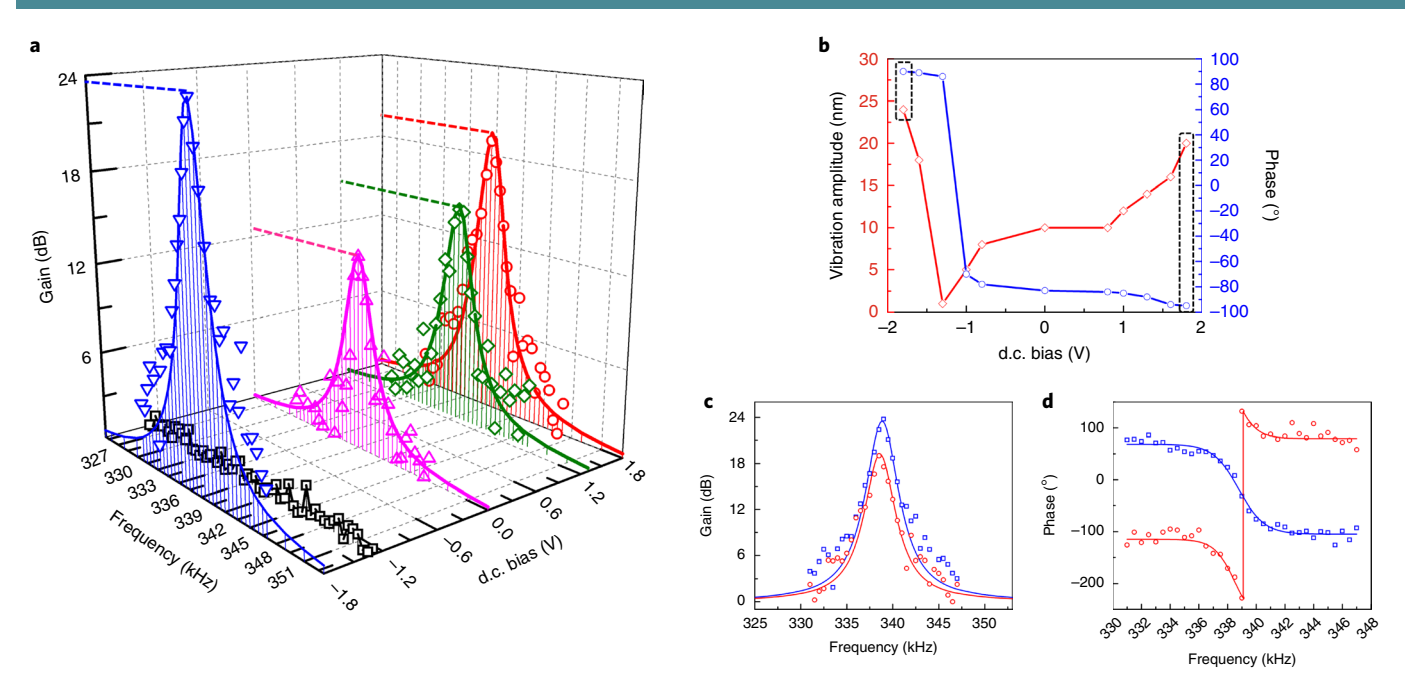


Fig. 4 | Time- and frequency-domain response of $Hf_{0.5}Zr_{0.5}O_2$ -transduced Si resonator for different ferroelectric polarization scenarios. **a**, The frequency response, around the out-of-plane flexural resonance mode, for various d.c. bias voltages (Lorentzian curves fitted on extracted data points). **b**, A summary of the resonance vibration amplitude and phase, for different d.c. bias voltages over the range from $-1.8\,\text{V}$ to $1.8\,\text{V}$. **c**, The vibration gain relative to the noise floor (Lorentzian curves fitted on extracted data points). **d**, The vibration phase of the resonator when the $Hf_{0.5}Zr_{0.5}O_2$ transducer is polarized by $1.8\,\text{V}$ (red line) and $-1.8\,\text{V}$ (blue line) d.c. bias voltages. The -180° difference in phase at resonance for the bias voltages of opposite sign elucidates the effect of polarization inversion on the electromechanical transduction (solid curves used as a guide to the eye to illustrate the phase change at resonance and the phase difference phenomenon).

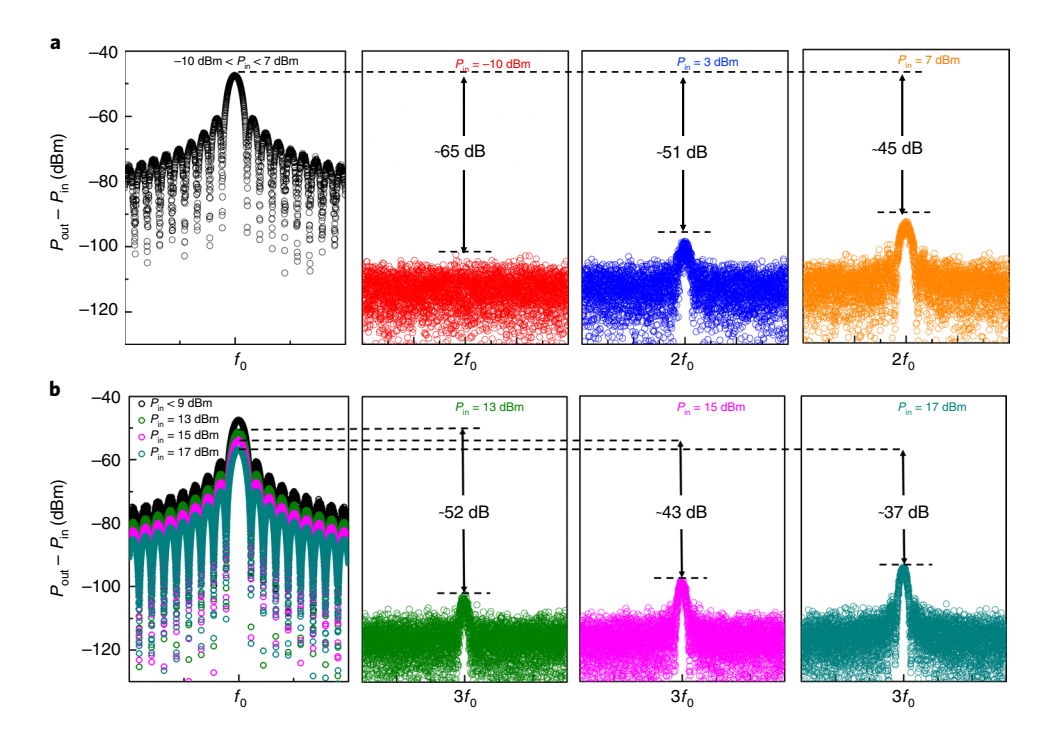


Fig. 5 | The output power spectrum around the fundamental, second and third harmonics for the $Hf_{0.5}Zr_{0.5}O_2$ -transduced AIN-on-Si resonator operating in lateral-extensional mode, for various input radio-frequency powers. a, The relative magnitude of the second harmonic, created from the electromechanical scattering caused by the nonlinear electrostrictive effect. b, The relative magnitude of the third harmonic generated by the thermomechanical nonlinearities. The magnitude of the fundamental harmonic is reduced by an increase in power when operating in the mechanically nonlinear regime, which corresponds to the distortion of the linear frequency response of the resonator and increased insertion loss at higher input powers.

ARTICLES NATURE ELECTRONICS

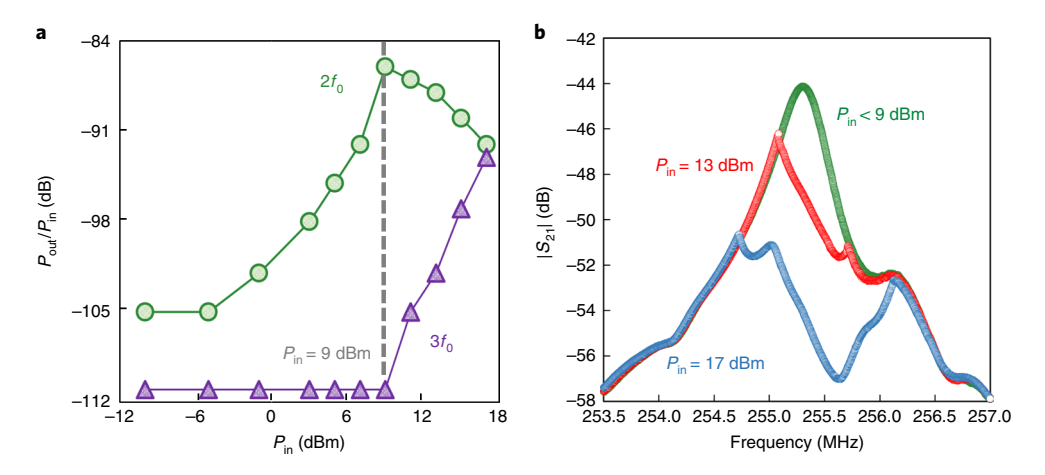


Fig. 6 | Comparison of electromechanical and thermomechanical scattering using fundamental, second and third harmonics. a, The relative magnitude of second (green circles) and third (purple triangles) harmonics over different electrical drive powers, when the $Hf_{0.5}Zr_{0.5}O_2$ -transduced AIN-on-Si resonator is excited in lateral-extensional mode. Below 9 dBm electrical input power, the electromechanical scattering due to the nonlinear electrostrictive effect induces the second harmonic with quadratically increasing magnitude. Beyond 9 dBm, thermomechanical nonlinearities induce large third harmonics that stand out from the noise floor. The reduction in second-harmonic magnitude beyond 9 dBm input power is due to distortion of the resonator frequency response, which increases the insertion loss at f_0 . **b**, The frequency response of the resonator when excited through the $Hf_{0.5}Zr_{0.5}O_2$ ferroelectric transducer and detected through the AIN piezoelectric transducer, for different input powers. Beyond the 9 dBm input power, the frequency response is distorted due to the rising thermomechanical nonlinearities.

 $-1.8\,\mathrm{V}$ to 1.8 V. Varying the d.c. bias changes the $\mathrm{Hf_{0.5}Zr_{0.5}O_2}$ polarization, in accordance with the polarization–electric-field loop shown in Fig. 1c, and results in a corresponding change in the vibration amplitude. Figure 4b summarizes the vibration amplitude and phase for various $V_{\mathrm{d.c.}}$ values. Specifically, Fig. 4c,d compares the frequency response of the resonator when biased at 1.8 V and $-1.8\,\mathrm{V}$ to elucidate the $\sim\!180^{\circ}$ phase shift in vibration dynamics when the polarization is reversed.

Effect of nonlinear electromechanical scattering

To further understand the effect of nonlinear electrostrictive transduction on device operation, the magnitudes of the second- and third-order harmonics are extracted while the device is excited at the mechanical resonance frequency with different radio-frequency powers. The nonlinear harmonic generation in electromechanical resonators is attributed to scattering, which refers to various nonlinear mechanisms in an electromechanical resonator that disperse the energy from the fundamental mode into higher-order harmonics. These mechanisms can be a result of nonlinear mechanical wavemixing processes that are induced by the elastic anharmonicity or temperature sensitivity of the resonator's constituent materials (that is, thermomechanical scattering) or induced by the nonlinear nature of the electromechanical transduction scheme that directly transfers a portion of electrical energy inserted into the resonator at f_0 into the Nf_0 harmonic, where N is an integer (that is, electromechanical scattering). While the thermomechanical scattering processes typically result in generation of the third-order harmonic, the electrostrictive effect in atomically engineered Hf_{0.5}Zr_{0.5}O₂ transducers scatters the electrical input into mechanical strain at twice the excitation frequency and yields second-order harmonic generation. To quantify the effect of electromechanical scattering and compare it with thermomechanical nonlinearities, the harmonic generation dynamics in the Hf_{0.5}Zr_{0.5}O₂-transduced AlN-on-Si resonator are studied. The resonator is excited using the $Hf_{0.5}Zr_{0.5}O_2$ transducer, with different electrical input powers over the range from −12 dBm to 18 dBm, and the AlN piezoelectric transducer is used to sense mechanical vibrations at the output port. Figure 5 shows the output power spectrum around the fundamental, second and third

harmonics for an ${\rm Hf_{0.5}Zr_{0.5}O_2}$ -transduced AlN-on-Si resonator that is excited in the lateral-extensional vibration mode at 255.5 MHz. For input powers below 9 dBm, the third-order harmonic remains below the noise floor at -112 dBm, confirming operation of the device in the linear thermomechanical regime. However, the power of the second-order harmonic increases with the increase in input radiofrequency power. In contrast, as the input power exceeds 9 dBm, the magnitude of the fundamental harmonic starts to decrease and the third harmonic stands out from the noise floor, with an increasing trend following the input power. This behaviour corresponds to the dominant contribution of thermomechanical nonlinearities that distort the resonator's linear transfer function and give rise to third-harmonic generation^{29–33}.

Figure 6 summarizes the second- and third-harmonic magnitudes over a wide range of input powers, highlighting different regimes of nonlinear scattering dominated by electromechanical and thermomechanical anharmonicities. For electrical excitations at the mechanical resonance with input powers below 9 dBm, the resonator operates in the linear mechanical regime. However, the electromechanical scattering induced by the electrostrictive effect in the $Hf_{0.5}Zr_{0.5}O_2$ transducer results in excitation of the second harmonic with quadratically proportional power. This result qualitatively follows the analytical derivations that quantify the relative ratio of linear and nonlinear mechanical strain excited with the application of electric field across the film thickness and through the electrostrictive effect by (see Supplementary Section 2 for further details)

$$\begin{array}{l} \begin{array}{l} {\rm nonlinearly\ scattered\ mechanical\ energy} \\ \overline{\ linearly\ transduced\ mechanical\ energy} \end{array} \propto \left(\frac{\varepsilon_{\rm nonlinear}}{\varepsilon_{\rm linear}}\right)^2 \\ = \frac{E_{\rm a.c.}^2}{4P_0^2} \left(1 + \frac{\epsilon_3'}{\epsilon_3} E_{\rm a.c.} + \frac{\epsilon_3'}{\epsilon_3} E_{\rm a.c.}^2 + \dots \right)^2 \end{array} \eqno(2)$$

Here, $\varepsilon_{\rm linear}$ and $\varepsilon_{\rm nonlinear}$ are the linear and nonlinear strain excited by application of the electric field $E_{\rm a.c.}$ to the transducer, P_0 is the instantaneous polarization at zero electric field and ε_3 and ε_3' are the first- and second-order dielectric constants of the transducer film. Beyond 9 dBm, the input electrical signal drives the resonator

NATURE ELECTRONICS ARTICLES

into thermomechanical nonlinearities, which gives rise to the thirdharmonic generation with a linearly increasing power. Figure 6b demonstrates the two-port transmission response of the resonator for various input powers, confirming the distortion in linear transfer function of the resonator due to the thermomechanical nonlinearities at input powers beyond 9dBm. It is also evident that the distortion in frequency response increases the insertion loss at the resonance frequency, which translates into an increase in device impedance at f_0 and induces a reduction in the relative power of the electromechanically generated second harmonic, as evident in Fig. 6a. Therefore, the experiment confirms the contribution of the electrostrictive effect to nonlinear scattering and harmonic generation in Hf_{0.5}Zr_{0.5}O₂-transduced resonators. While the nonlinear electromechanical scattering resulting from the electrostrictive effect in atomically engineered Hf_{0.5}Zr_{0.5}O₂ transducers degrades the resonator performance in the mechanically linear regime, it provides promising potential for nonlinear mode-coupling in nanosystems^{34–36} or realization of nonlinear nanoacoustic and nonreciprocal components³⁷⁻³⁹, especially at centimetre- and millimetre-wave frequencies.

Conclusions

We have reported integrated nanoelectromechanical transducers created from 10 nm ferroelectric Hf_{0.5}Zr_{0.5}O₂ films. The transducers, integrated on single-crystal Si and AlN-on-Si membranes, provide high-Q nanomechanical resonators operating over the 340 kHz to 13 GHz frequency range and in flexural and extensional vibration modes. The 13 GHz device demonstrated a figure of merit of $f_0Q \approx 3.97 \times 10^{12}$, which is the highest reported for any nanomechanical resonator operating in the centimetre-wave regime. We also clarified the role of the electrostrictive effect in the electromechanical transduction of the Hf_{0.5}Zr_{0.5}O₂ transducers, which allows precise control of the resonator vibration amplitude and phase through variation of the ferroelectric polarization via the bias voltage. Furthermore, we demonstrated the contribution of the nonlinear electrostrictive effect to the electromechanical scattering of the resonator energy into the second-harmonic signal. Comparison of the magnitudes of the electro- and thermomechanical scattering over a range of electric input power confirms the large contribution of the electromechanical scattering in Hf_{0.5}Zr_{0.5}O₂ resonators operating in the linear thermomechanical regime and highlights the potential of this material for making nanomechanical resonators for application in extreme frequency scaling, wideband frequency combs and integrated nonlinear-non-reciprocal spectral processors.

Methods

Device fabrication. The $Hf_{0.5}Zr_{0.5}O_2$ nanoelectromechanical transducers are realized through atomic layer deposition, stacking with a TiN layer and proper RTA. The nanomechanical resonators are fabricated by integration of $Hf_{0.5}Zr_{0.5}O_2$ films on Si and AlN-on-Si membranes, followed by various etching and deposition processes to create free-standing devices and electrical pads for application of excitation and sensing signals (see Supplementary Section 1A for fabrication and processing details).

Device characterization. $Hf_{0.5}Zr_{0.5}O_2$ films are electrically measured with a modified Sawyer–Tower circuit to extract the polarization–electric-field hysteresis characteristic corresponding to ferroelectric behaviour. Nanomechanical resonators with integrated $Hf_{0.5}Zr_{0.5}O_2$ transducers are electrically characterized using a Keysight N5222A network analyser, Keysight E5173B signal generator and Keysight N9010A signal analyser, to extract the frequency response and characterize the magnitude of nonlinearly generated harmonics. The $Hf_{0.5}Zr_{0.5}O_2$ -transduced Si nanomechanical resonator is optically characterized using a Lyncée Tec R-2100 series reflection digital holographic microscope that is synchronized with a stroboscopic signal generator (see Supplementary Section 1C for device characterization details).

 ${\bf SEM.}$ SEM images are taken using a FEI Nova NanoSEM 430 system.

TEM. TEM images are taken using a FEI TECNAI F20 S/TEM system.

Electrostrictive effect formulation. The electromechanical transduction based on the electrostrictive effect in ferroelectric materials can be formulated through polynomial approximation of the polarization–electric-field characteristic. Two regimes of operation, linear and nonlinear, can be identified depending on the electric field excitation amplitude and applied d.c. bias voltage (see Supplementary Section 2 for further details).

Data availability

The authors declare that the main data supporting the findings of this study are available within the article and its Supplementary Information. Extra data are available from the corresponding author on request.

Received: 28 March 2019; Accepted: 20 August 2019; Published online: 7 October 2019

References

- 1. LaHaye, M. D., Buu, O., Camarota, B. & Schwab, K. C. Approaching the quantum limit of a nanomechanical resonator. *Science* **304**, 74–77 (2004).
- Jensen, K., Kim, K. & Zettl, A. An atomic-resolution nanomechanical mass sensor. Nat. Nanotechnol. 3, 533 (2008).
- 3. Barson, M. S. et al. Nanomechanical sensing using spins in diamond. *Nano Lett.* **17**, 1496–1503 (2017).
- Ramezany, A. & Pourkamali, S. Ultrahigh frequency nanomechanical piezoresistive amplifiers for direct channel-selective receiver front-ends. Nano Lett. 18, 2551–2556 (2018).
- Villanueva, L. G. et al. A nanoscale parametric feedback oscillator. Nano Lett. 11, 5054–5059 (2011).
- Naing, T. L., Rocheleau, T. O., Ren, Z., Li, S. S. & Nguyen, C. T. C. High-Q UHF spoke-supported ring resonators. J. Microelectromech. Syst. 25, 11–29 (2016).
- Pourkamali, S., Ho, G. K. & Ayazi, F. Low-impedance VHF and UHF capacitive silicon bulk acoustic wave resonators—part I: concept and fabrication. *IEEE Trans. Electron Devices* 54, 2017–2023 (2007).
- Ruby, R. et al. Positioning FBAR technology in the frequency and timing domain. *IEEE Trans. Ultrason. Ferroelectr. Freq. Control* 59, 334–345 (2012).
- Cassella, C. et al. Super high frequency aluminum nitride two-dimensional-mode resonators with k_i² exceeding 4.9%. *IEEE Microw. Wirel. Compon. Lett.* 27, 105–107 (2017).
- Iborra, E., Clement, M., Capilla, J., Olivares, J. & Felmetsger, V. Low-thickness high-quality aluminum nitride films for super high frequency solidly mounted resonators. *Thin Solid Films* 520, 3060–3063 (2012).
- Sinha, N., et al. Ultra thin AlN piezoelectric nano-actuators. In TRANSDUCERS 2009—2009 International Solid-State Sensors, Actuators and Microsystems Conference 469–472 (IEEE, 2009).
- Wang, Z. et al. Black phosphorus nanoelectromechanical resonators vibrating at very high frequencies. Nanoscale 7, 877–884 (2015).
- Lee, J., Wang, Z., He, K., Shan, J. & Feng, P. X. L. High frequency MoS₂ nanomechanical resonators. ACS Nano 7, 6086–6091 (2013).
- 14. Bunch, J. S. et al. Electromechanical resonators from graphene sheets. *Science* **315**, 490–493 (2007).
- Chen, C. Y. et al. Performance of monolayer graphene nanomechanical resonators with electrical readout. Nat. Nanotechnol. 4, 861–867 (2009).
- van der Zande, A. M. et al. Large-scale arrays of single layer graphene resonators. Nano Lett. 10, 4869–4873 (2010).
- Eichler, A. et al. Nonlinear damping in mechanical resonators made from carbon nanotubes and graphene. Nat. Nanotechnol. 6, 339–342 (2011).
- 18. Böscke, T. S., Müller, J., Bräuhaus, D., Schröder, U. & Böttger, U. Ferroelectricity in hafnium oxide thin films. *Appl. Phys. Lett.* **99**, 102903
- Mulaosmanovic, H. et al. Switching kinetics in nanoscale hafnium oxide based ferroelectric field-effect transistors. ACS Appl. Mater. Interfaces 9, 3792–3798 (2017).
- Chernikova, A. et al. Ultrathin Hf_{0.5}Zr_{0.5}O₂ ferroelectric films on Si. ACS Appl. Mater. Interfaces 8, 7232–7237 (2016).
- Ghatge, M., Walters, G., Nishida, T., & Tabrizian, R. A nano-mechanical resonator with 10nm hafnium-zirconium oxide ferroelectric transducer. In 2018 IEEE International Electron Devices Meeting (IEDM) 4–6 (IEEE, 2019).
- Böscke, T. S. et al. Phase transitions in ferroelectric silicon doped hafnium oxide. Appl. Phys. Lett. 99, 112904 (2011).
- Park, M. H. et al. Evolution of phases and ferroelectric properties of thin Hf_{0.5}Zr_{0.5}O₂ films according to the thickness and annealing temperature. Appl. Phys. Lett. 102, 242905 (2013).
- 24. Park, M. H. et al. Ferroelectricity and antiferroelectricity of doped thin $\rm HfO_2$ -based films. *Adv. Mater.* 27, 1811–1831 (2015).
- Park, M. H. et al. Toward a multifunctional monolithic device based on pyroelectricity and the electrocaloric effect of thin antiferroelectric Hf_xZr_{1-x}O₂ films. Nano Energy 12, 131–140 (2015).

ARTICLES NATURE ELECTRONICS

- Materlik, R., Künneth, C. & Kersch, A. The origin of ferroelectricity in Hf_{1-x}Zr_xO₂: a computational investigation and a surface energy model. *J. Appl. Phys.* 117, 134109 (2015).
- Schroeder, U. et al. Impact of different dopants on the switching properties of ferroelectric hafnium oxide. *Jpn. J. Appl. Phys.* 53, 08LE02 (2014).
- 28. Sundar, V. & Newnham, R. E. Electrostriction and polarization. *Ferroelectrics* 135, 431–446 (1992).
- Gieseler, J., Novotny, L. & Quidant, R. Thermal nonlinearities in a nanomechanical oscillator. Nat. Phys. 9, 806 (2013).
- Segovia-Fernandez, J. & Piazza, G. Thermal nonlinearities in contour mode AlN resonators. J. Microelectromech. Syst. 22, 976–985 (2013).
- Ghatge, M., Karri, P., & Tabrizian, R. Power-insensitive silicon crystal-cut for amplitude-stable frequency synthesis. In 2017 IEEE 30th International Conference on Micro Electro Mechanical Systems (MEMS) 76–79 (IEEE, 2017).
- 32. Polunin, P. M., Yang, Y., Dykman, M. I., Kenny, T. W. & Shaw, S. W. Characterization of MEMS resonator nonlinearities using the ringdown response. *J. Microelectromech. Syst.* **25**, 297–303 (2016).
- Rocas, E., Collado, C., Mateu, J., Campanella, H., & O'Callaghan, J. M. Third order intermodulation distortion in film bulk acoustic resonators at resonance and antiresonance. In 2008 IEEE MTT-S International Microwave Symposium Digest 1259–1262 (IEEE, 2008).
- Matheny, M. H., Villanueva, L. G., Karabalin, R. B., Sader, J. E. & Roukes, M. L. Nonlinear mode-coupling in nanomechanical systems. *Nano Lett.* 13, 1622–1626 (2013).
- Ghatge, M. & Tabrizian, R. Exploiting elastic anharmonicity in aluminum nitride matrix for phase-synchronous frequency reference generation. *Appl. Phys. Lett.* 112, 123503 (2018).
- Zhu, J., Ru, C. Q. & Mioduchowski, A. High-order subharmonic parametric resonance of multiple nonlinearly coupled micromechanical nonlinear oscillators. *Acta Mech.* 212, 69–81 (2010).
- Popa, B. I. & Cummer, S. A. Non-reciprocal and highly nonlinear active acoustic metamaterials. *Nat. Commun.* 5, 3398 (2014).

- 38. Lepri, S. & Pikovsky, A. Nonreciprocal wave scattering on nonlinear string-coupled oscillators. *Chaos* 24, 043119 (2014).
- Ghatge, M., Walters, G., Nishida, T. & Tabrizian, R. A non-reciprocal filter using asymmetrically transduced micro-acoustic resonators. *IEEE Electron Device Lett.* 40, 800–803 (2019).

Acknowledgements

We would like to thank the Nanoscale Research Facility at the University of Florida for the fabrication facilities and N. Rudawski for help with TEM. This work was supported in part by the NSF grants ECCS 1610387 and ECCS 1752206.

Author contributions

M.G. designed, fabricated and measured the resonators. G.W. fabricated and characterized the $Hf_{0.5}Zr_{0.5}O_2$ ferroelectric film. T.N. and R.T. supervised the project and provided guidance throughout the process. All authors participated in analysing the results and contributed to writing the manuscript. All authors have given approval to the final version of the manuscript.

Competing interests

The authors declare no competing interests.

Additional information

Supplementary information is available for this paper at https://doi.org/10.1038/s41928-019-0305-3.

Correspondence and requests for materials should be addressed to R.T.

Reprints and permissions information is available at www.nature.com/reprints.

Publisher's note Springer Nature remains neutral with regard to jurisdictional claims in published maps and institutional affiliations.

© The Author(s), under exclusive licence to Springer Nature Limited 2019